Wave-packet continuum-discretization approach to proton collisions with helium

Wave-packet continuum-discretization approach to proton collisions with helium

Sh. U. Alladustov, I. B. Abdurakhmanov, A. S. Kadyrov, and I. Bray
Curtin Institute for Computation and Department of Physics and Astronomy, Curtin University, GPO Box U1987, Perth, WA 6845, Australia

K. Bartschat
Department of Physics and Astronomy, Drake University, Des Moines, Iowa 50311, USA

(Received 14 March 2019; published 28 May 2019)

We extend the two-center wave-packet convergent close-coupling method to proton collisions with helium. The target is treated as a three-body system, where correlations between the electrons are taken into account. We apply a frozen-core approximation, where one of the electrons is described by the He^+ 1*s* orbital, and obtain the helium singlet wave functions as well as the energy levels using a numerical approach. The wave-packet approach is used to discretize the continuum of the target and the hydrogen atom formed after electron capture by the projectile. Convergence of the results is studied in terms of the included projectile- and target-centered states. We present electron-capture and single- and double-ionization cross sections for protons incident on He in the ground state in the energy range from 15 keV to 1 MeV. We also provide partial cross sections for electron capture and direct excitation into the $n = 2$ shell states of hydrogen and helium, respectively. Our results are in good agreement with available experimental data and other calculations, where available.

DOI: 10.1103/PhysRevA.99.052706

I. INTRODUCTION

The study of ion-atom collisions is one of the intensive research areas in atomic physics. A thorough understanding of ionization and charge-exchange phenomena in such collisions is essential for applications in a wide range of sciences such as astrophysics [1] and plasma physics [2]. Moreover, these processes are relevant to hadron therapy [3]. Collisions of protons with helium atoms have been investigated to a great extent both theoretically [4–32] and experimentally [33–49].

Various theoretical approaches were applied to investigate the four-body *p*-He system depending on the incident energy of the projectile. Zajfman and Maor [22] and Schultz and Lynn [15] used the classical trajectory Monte Carlo (CTMC) method to calculate the total electron-capture and single-ionization cross sections. Zajfman and Maor [22] achieved limited success in comparison with other works, while Schultz and Lynn [15] obtained reasonable agreement with available experimental data for projectile incident energies from 25 keV to 500 keV.

The first Born approximation (FBA) has also been used in high-energy ion-atom collisions, where coupling between channels can be neglected. Several versions of the FBA approach are known in the literature. In particular, for the proton-helium collision system, where the exact wave functions describing the helium target are not available, there exists the post-prior discrepancy of FBA. Mapleton [14] investigated prior and post forms of the Born approximation to calculate electron-capture cross sections in the *p*-He collisions. Belkić [6] developed the FBA with corrected boundary conditions (B1B) and used it at intermediate and high energies. The B1B approach to the *p*-He problem was based on an independent-particle model. The target was described using Roothaan-Hartree-Fock and hydrogenlike wave functions. Good agreement with the experiment was obtained at energies from 50 keV to 50 MeV when the Roothaan-Hartree-Fock wave functions were employed.

Another perturbative approach to the problem is based on the distorted-wave formalism. A number of distorted-wave theories were discussed by Toshima *et al.* [19]. Mancev *et al.* [13] and Jana *et al.* [11] used the four-body distorted-wave Born approximation (DWBA) method, while the three-body DWBA was employed in the recent work of Rahmanian *et al.* [16]. However, due to their nature, all of the available perturbative approaches become unreliable whenever the projectile speed is smaller than the classical speed of the orbiting electron of the target.

A number of sophisticated nonperturbative approaches attempted to address the latter energy regime. Zapukhlyak *et al.* [23] developed a nonperturbative basis-generator method. More recently, Baxter and Kirchner [5] developed a time-dependent density-functional theory (TDDFT) to calculate total cross sections for electron-capture and ionization processes in the proton-helium collisions. Correlation effects were taken into account using two different models: the integral model of Wilken and Bauer (WB) and an independent-electron model (IEM). A better agreement with the measurements was obtained using the WB model.

Another widely used high-order method for describing ion-atom collisions is the semiclassical close-coupling approach. In the close-coupling approach the choice of basis functions and the completeness of the basis are very important. A number of authors chose this method to investigate the *p*-He system. Winter [20] used 50 Sturmian functions as a basis to calculate electron-capture and ionization cross sections. However, he neglected electron exchange in the final transfer

channels. Somewhat similar 51-state calculations but with different basis functions were presented by Slim *et al.* [18], where electron exchange in the H-He^+ channel was taken into account. Both calculations failed to achieve a sufficient level of convergence.

There are several other approaches to the problem that need to be mentioned. The symmetric eikonal (SE) approximation is applicable at intermediate and high energies and was employed by Deco *et al.* [8]. In addition, there are the convergent frozen-correlation approximation (CFCA) by Díaz *et al.* [9], a unified atomic-orbital molecular-orbital matching method by Kimura and Lin [12] suitable for low energies, and the four-body boundary-corrected continuum-intermediate-state approximation by Samanta and Purkait [17]. All these calculations gave results that agree with the experiments quite well. However, their validity is limited to a particular energy region and/or a particular process involved in the collisions (e.g., electron capture).

A wave-packet convergent close-coupling (WP-CCC) approach to the four-body problem of antiproton-helium scattering was developed by Abdurakhmanov *et al.* [50]. The proton-helium system is more complicated than antiproton-helium due to the existence of the electron capture channel. It requires accounting for computationally demanding rearrangement channels that lead to hydrogen formation. In most of the works described above, the problem was reduced to a three-body one using some approximations, as the four-body problem is computationally very hard to solve.

In the present work we develop a four-body semiclassical close-coupling approach based on the wave-packet discretization, which was successfully applied to a single-center problem of antiproton-helium collisions [50]. To this end the full four-body Schrödinger equation is solved by expanding the total scattering wave function in a two-center basis of atomic wave functions. This leads to a set of coupled differential equations for the transition probability amplitudes, which are used to calculate the cross sections for elastic scattering, target excitation, and electron capture by the projectile and ionization. The wave functions representing atomic hydrogen are the true eigenfunctions for the negative-energy states and orthonormal stationary wave packets for positive-energy states. The wave packets representing the target continuum are constructed using the helium continuum functions, which were obtained by solving the Schrödinger equation describing the helium target numerically. Convergence of the predicted cross sections for various occurring processes is achieved by increasing the number of included negative-energy eigenstates and positive-energy pseudostates for the projectile-electron and target-electron systems. We investigate electron capture, direct excitation, and single and double ionization in the energy range from 15 keV to 1 MeV. We perform convergence studies in terms of the number of included basis functions.

This paper is structured as follows. In Sec. II we give a description of our two-center WP-CCC approach to the problem of proton-helium scattering. The details and the results of our calculations are presented in Secs. III and IV. Finally, in Sec. V we highlight the main findings and draw conclusions. Unless specified otherwise, atomic units are used throughout this manuscript.

II. THEORY

A. Coupled differential equations

Below we describe the extension of the single-center semiclassical convergent close-coupling (CCC) method [50] to the two-center problem of proton collisions with helium to include the electron-capture channels. We apply the frozen-core approximation, where one of the electrons of the helium atom remains in the $1s$ state of He^+ throughout the collision. For simplicity, we refer throughout this work to the channels of the active electron as helium channels, e.g., α channel of helium means that the active electron of helium is in the α channel. The total scattering wave function Ψ satisfies the exact time-independent Schrödinger equation

$$(H - E)\Psi = 0, \tag{1}$$

where H is the full four-body Hamiltonian and E is the total energy

$$E = E_0 + \frac{k_\alpha^2}{2\mu_1} + \epsilon_\alpha = E_0 + \frac{k_{1\beta}^2}{2\mu_2} + \epsilon_{1\beta} = E_0 + \frac{k_{2\beta}^2}{2\mu_2} + \epsilon_{2\beta}, \tag{2}$$

with E_0 being the binding energy of the frozen target electron. The index α denotes the full set of quantum numbers representing a state in the direct p-He channel. The index β denotes the same but in the rearrangement channel H-He^+, formed after the projectile captures the active electron of the target. Furthermore, $\boldsymbol{k}_\alpha$ is the momentum of the projectile relative to the helium atom in the α channel, μ_1 is the reduced mass of this system, and ϵ_α is the eigenenergy of the bound state α, $\boldsymbol{k}_{1\beta}$ (and $\boldsymbol{k}_{2\beta}$) is the momentum of the formed hydrogen atom relative to the residual helium ion in the 1β (2β) channel, μ_2 is the reduced mass, and $\epsilon_{1\beta}$ ($\epsilon_{2\beta}$) is the eigenenergy of hydrogen in the 1β (2β) channel. Channel 1β is the same as channel 2β but with the electron of the residual target and that of the hydrogen atom exchanged.

The total Hamiltonian H of the scattering system can be represented as sums of the kinetic-energy operators and Coulomb interaction potentials:

$$H = K_\sigma + H_{T_1} + H_{T_2} + V_P + V_{12}, \tag{3}$$

$$H = K_{\rho_1} + H_{P_1} + H_{T_2} + V_1 + V_{12}, \tag{4}$$

$$H = K_{\rho_2} + H_{P_2} + H_{T_1} + V_2 + V_{12}, \tag{5}$$

where

$$K_\sigma = -\frac{\nabla_{\boldsymbol{\sigma}}^2}{2\mu_1}, \quad K_{\rho_i} = -\frac{\nabla_{\boldsymbol{\rho}_i}^2}{2\mu_2}, \quad i = 1, 2 \tag{6}$$

and

$$V_P = \frac{2}{R} - \frac{1}{x_1} - \frac{1}{x_2}, \tag{7}$$

$$V_1 = \frac{2}{R} - \frac{2}{r_2} - \frac{1}{x_1}, \tag{8}$$

$$V_2 = \frac{2}{R} - \frac{2}{r_1} - \frac{1}{x_2}, \tag{9}$$

$$V_{12} = \frac{1}{|\boldsymbol{r}_1 - \boldsymbol{r}_2|}. \tag{10}$$

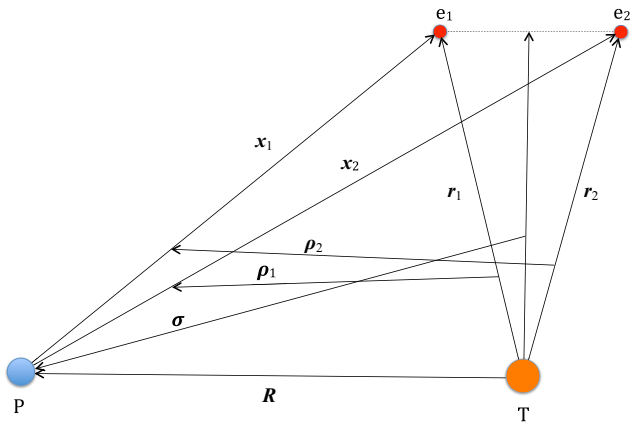

FIG. 1. Jacobi coordinates for the proton-helium system.

Here $\boldsymbol{R}$, $\boldsymbol{r}_1$, and $\boldsymbol{r}_2$ are the position vectors of the incident proton and the two electrons relative to the helium nucleus, $\boldsymbol{x}_1$ and $\boldsymbol{x}_2$ are the position vectors of the electrons relative to the incident proton, $\boldsymbol{\sigma}$ is the position vector of the proton relative to center of mass of the helium atom, and $\boldsymbol{\rho}_1$ ($\boldsymbol{\rho}_2$) is the position of the proton and the first (second) electron system relative to the helium ion (see Fig. 1). The Hamiltonians of the hydrogen atom and the He^+ ion formed by each of the target electrons are written as

$$H_{P_i} = -\frac{\nabla^2_{\boldsymbol{x}_i}}{2} - \frac{1}{x_i}, \quad i = 1, 2, \tag{11}$$

$$H_{T_i} = -\frac{\nabla^2_{\boldsymbol{r}_i}}{2} - \frac{2}{r_i}, \quad i = 1, 2, \tag{12}$$

respectively. With these definitions the Hamiltonian of the helium atom is written as

$$H_T = H_{T_1} + H_{T_2} + V_{12}. \tag{13}$$

In our model the target nucleus is located at the origin, and we assume that the projectile is moving along a classical trajectory $\boldsymbol{R} \equiv \boldsymbol{R}(t) = \boldsymbol{b} + \boldsymbol{v}t$, where $\boldsymbol{b}$ is the impact parameter and $\boldsymbol{v}$ is the initial velocity of the projectile relative to the target. The vector $\boldsymbol{b}$ is perpendicular to the direction of the moving proton, i.e., $\boldsymbol{b} \cdot \boldsymbol{v} = 0$.

We assume that the total electronic spin of helium is conserved in the collision process. Then the total scattering wave function is expanded in terms of N target-centered and M projectile-centered pseudostates as

$$\Psi = \sum_{\alpha=1}^{N} a_\alpha(t, \boldsymbol{b}) \psi^{\mathrm{He}}_\alpha(\boldsymbol{r}_1, \boldsymbol{r}_2) e^{i\boldsymbol{k}_\alpha \boldsymbol{\sigma}} + \frac{1}{\sqrt{2}} \sum_{\beta=1}^{M} b_\beta(t, \boldsymbol{b}) \times \left[\psi^{\mathrm{H}}_\beta(\boldsymbol{x}_1) \psi^{\mathrm{He}^+}_{1s}(\boldsymbol{r}_2) e^{i\boldsymbol{k}_{1\beta}\boldsymbol{\rho}_1} + \psi^{\mathrm{H}}_\beta(\boldsymbol{x}_2) \psi^{\mathrm{He}^+}_{1s}(\boldsymbol{r}_1) e^{i\boldsymbol{k}_{2\beta}\boldsymbol{\rho}_2}\right], \tag{14}$$

where $\psi^{\mathrm{He}}_\alpha$ and ψ^{H}_β are the wave functions for helium and hydrogen, respectively, and $\psi^{\mathrm{He}^+}_{1s}$ is the ground-state wave function for He^+. Their detailed definitions will be given below. The expansion coefficients $a_\alpha(t, \boldsymbol{b})$ and $b_\alpha(t, \boldsymbol{b})$ at $t \to +\infty$ represent the transition amplitudes into the various target and projectile states.

We substitute the expansion (14) into Eq. (1) and take into account the relationships

$$\nabla_{\boldsymbol{\sigma}} e^{i\boldsymbol{k}_\alpha \boldsymbol{\sigma}} = i\boldsymbol{k}_\alpha e^{i\boldsymbol{k}_\alpha \boldsymbol{\sigma}}, \quad \nabla^2_{\boldsymbol{\sigma}} e^{i\boldsymbol{k}_\alpha \boldsymbol{\sigma}} = -k^2_\alpha e^{i\boldsymbol{k}_\alpha \boldsymbol{\sigma}}, \tag{15}$$

$$\nabla_{\boldsymbol{\rho}_1} e^{i\boldsymbol{k}_{1\beta}\boldsymbol{\rho}_1} = i\boldsymbol{k}_{1\beta} e^{i\boldsymbol{k}_{1\beta}\boldsymbol{\rho}_1}, \quad \nabla^2_{\boldsymbol{\rho}_1} e^{i\boldsymbol{k}_{1\beta}\boldsymbol{\rho}_1} = -k^2_\beta e^{i\boldsymbol{k}_{1\beta}\boldsymbol{\rho}_1}, \tag{16}$$

$$\nabla_{\boldsymbol{\rho}_2} e^{i\boldsymbol{k}_{2\beta}\boldsymbol{\rho}2} = i\boldsymbol{k}_{2\beta} e^{i\boldsymbol{k}_{2\beta}\boldsymbol{\rho}_2}, \quad \nabla^2_{\boldsymbol{\rho}_2} e^{i\boldsymbol{k}_{2\beta}\boldsymbol{\rho}_2} = -k^2_\beta e^{i\boldsymbol{k}_{2\beta}\boldsymbol{\rho}_2}, \tag{17}$$

and

$$\frac{\boldsymbol{k}_\alpha}{\mu_1} \nabla_{\boldsymbol{\sigma}} = \frac{\partial}{\partial t}, \quad \frac{\boldsymbol{k}_{1\beta}}{\mu_2} \nabla_{\boldsymbol{\rho}_1} = \frac{\partial}{\partial t}, \quad \frac{\boldsymbol{k}_{2\beta}}{\mu_2} \nabla_{\boldsymbol{\rho}_2} = \frac{\partial}{\partial t}. \tag{18}$$

Since the coefficients a_α and b_β vary slowly with t, the terms $\nabla^2_{\boldsymbol{\sigma}} a_\alpha$, $\nabla^2_{\boldsymbol{\rho}_1} b_\beta$, and $\nabla^2_{\boldsymbol{\rho}_2} b_\beta$ are very small and can be neglected. Then we successively multiply all terms of the resulting equation by $\psi^{\mathrm{He}*}_{\alpha'}(\boldsymbol{r}_1, \boldsymbol{r}_2) e^{-i\boldsymbol{k}_{\alpha'}\boldsymbol{\sigma}}$ for $\alpha' = 1, \ldots, N$ and $\psi^{\mathrm{H}*}_{\beta'}(\boldsymbol{x}_1) \psi^{\mathrm{He}^+}_{1s}(\boldsymbol{r}_2) e^{-i\boldsymbol{k}_{1\beta'}\boldsymbol{\rho}_1} + \psi^{\mathrm{H}*}_{\beta'}(\boldsymbol{x}_2) \psi^{\mathrm{He}^+}_{1s}(\boldsymbol{r}_1) e^{-i\boldsymbol{k}_{2\beta'}\boldsymbol{\rho}_2}$ for $\beta' = 1, \ldots, M$. After integrating over all variables except for $\boldsymbol{\sigma}$, $\boldsymbol{\rho}_1$, and $\boldsymbol{\rho}_2$, we obtain a set of coupled first-order differential equations for the time-dependent coefficients:

$$i\dot{a}_{\alpha'} + i \sum_{\beta=1}^{M} \dot{b}_\beta K^T_{\alpha'\beta} = \sum_{\alpha=1}^{N} a_\alpha D^T_{\alpha'\alpha} + \sum_{\beta=1}^{M} b_\beta Q^T_{\alpha'\beta},$$

$$i \sum_{\alpha=1}^{N} \dot{a}_\alpha K^P_{\beta'\alpha} + i \sum_{\beta=1}^{M} \dot{b}_\beta L^P_{\beta'\beta} = \sum_{\alpha=1}^{N} a_\alpha Q^P_{\beta'\alpha} + \sum_{\beta=1}^{M} b_\beta D^P_{\beta'\beta},$$

$$\alpha' = 1, 2, \ldots, N, \quad \beta' = 1, 2, \ldots, M. \tag{19}$$

Here the direct matrix elements have the forms

$$L^P_{\beta'\beta} = \frac{1}{2} \sum_{i,j=1,2} \left\langle \boldsymbol{k}_{i\beta'}, \psi^{\mathrm{H}}_{\beta'}, \psi^{\mathrm{He}^+}_{1s} \middle| \psi^{\mathrm{H}}_\beta, \psi^{\mathrm{He}^+}_{1s}, \boldsymbol{k}_{j\beta} \right\rangle, \tag{20}$$

$$D^T_{\alpha'\alpha} = \left\langle \boldsymbol{k}_{\alpha'}, \psi^{\mathrm{He}}_{\alpha'} \middle| H_T - E^{\mathrm{He}}_\alpha + V_P \middle| \psi^{\mathrm{He}}_\alpha, \boldsymbol{k}_\alpha \right\rangle, \tag{21}$$

$$D^P_{\beta'\beta} = \frac{1}{2} \sum_{i,j=1,2} \left\langle \boldsymbol{k}_{i\beta'}, \psi^{\mathrm{H}}_{\beta'}, \psi^{\mathrm{He}^+}_{1s} \middle| H_{Pi} - \varepsilon^{\mathrm{H}}_\beta \middle| \psi^{\mathrm{H}}_\beta, \psi^{\mathrm{He}^+}_{1s}, \boldsymbol{k}_{j\beta} \right\rangle + \frac{1}{2} \sum_{i,j=1,2} \left\langle \boldsymbol{k}_{i\beta'}, \psi^{\mathrm{H}}_{\beta'}, \psi^{\mathrm{He}^+}_{1s} \middle| V_i \middle| \psi^{\mathrm{H}}_\beta, \psi^{\mathrm{He}^+}_{1s}, \boldsymbol{k}_{j\beta} \right\rangle. \tag{22}$$

For the rearrangement matrix elements we have

$$K^P_{\beta'\alpha} = \frac{1}{\sqrt{2}} \sum_{i=1,2} \left\langle \boldsymbol{k}_{i\beta'}, \psi^{\mathrm{H}}_{\beta'}, \psi^{\mathrm{He}^+}_{1s} \middle| \psi^{\mathrm{He}}_\alpha, \boldsymbol{k}_\alpha \right\rangle, \tag{23}$$

$$K^T_{\alpha'\beta} = \frac{1}{\sqrt{2}} \sum_{i=1,2} \left\langle \boldsymbol{k}_{\alpha'}, \psi^{\mathrm{He}}_{\alpha'} \middle| \psi^{\mathrm{H}}_\beta, \psi^{\mathrm{He}^+}_{1s}, \boldsymbol{k}_{i\beta} \right\rangle, \tag{24}$$

$$Q^P_{\beta'\alpha} = \frac{1}{\sqrt{2}} \sum_{i=1,2} \left\langle \boldsymbol{k}_{i\beta'}, \psi^{\mathrm{H}}_{\beta'}, \psi^{\mathrm{He}^+}_{1s} \middle| H_T - E^{\mathrm{He}}_\alpha + V_P \middle| \psi^{\mathrm{He}}_\alpha, \boldsymbol{k}_\alpha \right\rangle, \tag{25}$$

$$Q^T_{\alpha'\beta} = \frac{1}{\sqrt{2}} \sum_{i=1,2} \left\langle \boldsymbol{k}_{\alpha'}, \psi^{\mathrm{He}}_{\alpha'} \middle| H_{Pi} - \varepsilon^{\mathrm{H}}_\beta + V_i \middle| \psi^{\mathrm{H}}_\beta, \psi^{\mathrm{He}^+}_{1s}, \boldsymbol{k}_{i\beta} \right\rangle. \tag{26}$$

We will return to the explicit calculations of the matrix elements in Sec. II C after defining the wave functions for the helium and hydrogen pseudostates.

The above system of equations is solved subject to the initial boundary condition

$$\begin{aligned} a_\alpha(-\infty, \boldsymbol{b}) &= \delta_{\alpha,1s}, \quad \alpha = 1, \ldots, N, \\ b_\beta(-\infty, \boldsymbol{b}) &= 0, \quad \beta = 1, \ldots, M, \end{aligned} \tag{27}$$

which assume that the active target electron is initially in the $1s$ orbital.

B. Structure of the hydrogen and helium atoms

1. Hydrogenic wave functions

As mentioned earlier, the projectile-centered states are described as products of wave functions of hydrogen and the ground-state wave function of He^+. The latter is described analytically as

$$\psi_{1s}^{\mathrm{He}^+}(\boldsymbol{r}) = \sqrt{\frac{2}{\pi}} r\, e^{-2r}. \tag{28}$$

To investigate double ionization of helium, we also need to define the entire set of wave functions for the helium ion. Below we describe the wave functions of a hydrogenlike atom of arbitrary charge Z.

Each state β is described by three quantum numbers $\{n, l, m\}$: the principal, orbital, and magnetic quantum numbers, respectively. For negative-energy states, the wave functions are separated into radial and angular parts as

$$\psi_\beta^{(Z)}(\boldsymbol{r}) = \phi_{nl}^{(Z)}(r) Y_{lm}(\hat{\boldsymbol{r}}) \tag{29}$$

and for positive-energy states as

$$\psi_\beta^{(Z)}(\boldsymbol{r}) = \sqrt{\frac{2}{\pi}} \sum_{lm} i^l \exp(-i\eta_l) R_{\kappa l}^{(Z)}(r) Y_{lm}^*(\hat{\boldsymbol{\kappa}}) Y_{lm}(\hat{\boldsymbol{r}}), \tag{30}$$

where Y_{lm} are spherical harmonics, $\kappa = \sqrt{2\varepsilon}$ is the momentum of the continuum state, with ε being the energy of the state and η_l the Coulomb phase shift.

The corresponding orthonormal radial wave functions are written analytically as

$$\phi_{nl}^{(Z)}(r) = \sqrt{Z \frac{(n-l-1)!}{(n+l)!}} e^{-Zr/n} \frac{(2Zr)^{l+1}}{n^{2+l}} L_{n-l-1}^{2l+1}\left(\frac{2Zr}{n}\right), \tag{31}$$

where L_{n-l-1}^{2l+1} denotes an associated Laguerre polynomial. For positive energies the corresponding continuum radial wave functions are given as

$$\begin{aligned} R_{\kappa l}^{(Z)}(r) = {} & \frac{1}{\sqrt{2\pi}} (2\kappa r)^{l+1} \exp\left(\frac{Z\pi}{2\kappa}\right) \frac{|\Gamma(l+1-iZ/\kappa)|}{(2l+1)!} \\ & \times e^{-i\kappa r}\, {}_1F_1\left(\frac{iZ}{\kappa} + l + 1, 2l+2, 2irk\right), \end{aligned} \tag{32}$$

where ${}_1F_1$ is a confluent hypergeometric function. These functions are not square integrable, and therefore not suitable for the close-coupling approach. To overcome this problem we use a wave-packet method [51]. In our work the wave packets are constructed as

$$\phi_{il}^{(Z)}(r) = \frac{1}{\sqrt{w_i}} \int_{\kappa_{i-1}}^{\kappa_i} d\kappa\, R_{\kappa l}^{(Z)}(r), \tag{33}$$

where

$$w_i = \kappa_i - \kappa_{i-1}, \tag{34}$$

with $\kappa_i = \sqrt{2\mathcal{E}_i}$. Nonoverlapping intervals $[\mathcal{E}_{i-1}, \mathcal{E}_i]_{i=1}^{N_c}$ divide the interval $[0, E_{\max}]$ into N_c subintervals, where $E_{\max}$ is the maximum allowed energy of the ejected electron. The intervals $[\mathcal{E}_{i-1}, \mathcal{E}_i]_{i=1}^{N_c}$ are called discretization bins, with N_c as the number of bins.

The wave packets constructed in this way are orthonormal and, together with the eigenstates, they form a basis to describe the hydrogenlike atom of charge Z. For the wave functions of hydrogen (i.e., when $Z = 1$) we use the notation ψ^{H} instead of $\psi^{(1)}$.

2. Helium wave functions

The target description is more complicated in this case, since we have a two-electron system and electron-electron correlation as well as electron exchange effects must be incorporated. The Schrödinger equation for this system cannot be solved analytically. Therefore, a numerical approach needs to be developed to find the solutions. Various existing theoretical works revealed that a careful choice of the helium wave functions is important in dealing with collisions of ions with the helium atom. Especially in the close-coupling approach they should be defined very accurately to obtain good convergence. In the present work we use the wave-packet-based description of the helium atom in the frozen-core approximation developed in [50]. Assuming that the total electronic spin of He, $S = 0$, is conserved during the collision, we write the wave function in the symmetric form

$$\psi_\alpha^{\mathrm{He}}(\boldsymbol{r}_1, \boldsymbol{r}_2) = \psi_\alpha(\boldsymbol{r}_1)\psi_{1s}^{(Z)}(\boldsymbol{r}_2) + \psi_\alpha(\boldsymbol{r}_2)\psi_{1s}^{(Z)}(\boldsymbol{r}_1), \tag{35}$$

where $\psi_{1s}^{(Z)}$ is the $1s$ orbital of the hydrogenlike atom of nuclear charge Z given in (31). This is a generalization of the wave function used by Abdurakhmanov *et al.* [50], where we set $Z = 2$ to correspond to the ground-state wave functions of He^+.

To obtain the functions ψ_α for each state α, we numerically solve the Schrödinger equation for helium

$$H_T \psi_\alpha^{\mathrm{He}}(\boldsymbol{r}_1, \boldsymbol{r}_2) = E_\alpha \psi_\alpha^{\mathrm{He}}(\boldsymbol{r}_1, \boldsymbol{r}_2), \tag{36}$$

where E_α is the total energy of the state α. Solutions of this equation depend on the parameter Z. We choose Z in a way that the total ground-state energy of the helium atom is equal to the experimental value of -2.904 a.u. [52]. Substituting the expansion (35) of the helium wave functions into Eq. (36), then projecting the result onto $\psi_{1s}^{(Z)}$, and taking into account $\langle \psi_{1s}^{(Z)} | \psi_{1s}^{(Z)} \rangle = 1$, we obtain the following integro-differential equation for ψ_α:

$$\begin{aligned} & \left[\nabla_{\boldsymbol{r}_1}^2 - 2V_1(r_1) + 2\varepsilon_\alpha + 2(2-z)V_2\right]\psi_\alpha(\boldsymbol{r}_1) + \left(2\varepsilon_\alpha + \frac{2(2-z)}{r_1}\right)\left\langle \psi_{1s}^{(Z)} \middle| \psi_\alpha \right\rangle \psi_{1s}^{(Z)}(\boldsymbol{r}_1) \\ & + \left\langle \psi_{1s}^{(Z)} \middle| \nabla_{\boldsymbol{r}_2}^2 + \frac{4}{r_2} \middle| \psi_\alpha \right\rangle_{\boldsymbol{r}_1} \psi_{1s}^{(Z)}(\boldsymbol{r}_1) - 2\left\langle \psi_{1s}^{(Z)} \middle| \frac{1}{|\boldsymbol{r}_1 - \boldsymbol{r}_2|} \middle| \psi_\alpha \right\rangle_{\boldsymbol{r}_1} \psi_{1s}^{(Z)}(\boldsymbol{r}_1) = 0, \end{aligned} \tag{37}$$

where

$$V_1(r_1) = -2/r_1 + \left\langle \psi_{1s}^{(Z)} \right| \frac{1}{|\boldsymbol{r}_1 - \boldsymbol{r}_2|} \left| \psi_{1s}^{(Z)} \right\rangle_{\boldsymbol{r}_1} \tag{38}$$

is the Hartree potential for an electron in a hydrogenlike ion of charge Z, and

$$V_2 = \left\langle \psi_{1s}^{(Z)} \right| \frac{1}{r_2} \left| \psi_{1s}^{(Z)} \right\rangle = \int_0^\infty \psi_{1s}^{(Z)}(r_2) \frac{1}{r_2} \psi_{1s}^{(Z)}(r_2) dr_2. \tag{39}$$

Separating the radial and angular parts of the wave functions for both negative- and positive-energy states, we obtain from Eq. (37) the following equation for the radial function $R_\alpha(r)$:

$$\frac{d^2 R_\alpha(r)}{dr^2} - \left[\frac{l(l+1)}{r^2} - \frac{4}{r} + 2W_0\left[\psi_{1s}^{(Z)}, \psi_{1s}^{(Z)}\right] - 2\varepsilon_\alpha - 2(2-z)V_2 \right] R_\alpha(r)$$
$$= \left[\frac{2}{2l+1} W_l\left[\psi_{1s}^{(Z)}, R_\alpha\right] - 2\int_0^\infty \psi_{1s}^{(Z)}(t) W_0[\psi_{1s}^{(Z)}, \psi_{1s}^{(Z)}] R_\alpha(t) dt - \left(2\varepsilon_\alpha + \frac{2(2-z)}{r}\right) \int_0^\infty \psi_{1s}^{(Z)}(t) R_\alpha(t) dt \right] \psi_{1s}^{(Z)}(r), \tag{40}$$

where

$$W_l[f, g] = \frac{1}{r^{l+1}} \int_0^r f(t) g(t) t^l dt + r^l \int_r^\infty \frac{f(t) g(t)}{t^{l+1}} dt. \tag{41}$$

We use an iterative approach to solve Eq. (40), where the Numerov method is applied in each iteration to find solutions of the linear inhomogeneous second-order differential equation for $R_\alpha^{(i)}(r)$. $R_\alpha^{(0)}(r)$ is found by replacing the right-hand side of Eq. (40) with zero. To ensure sufficient accuracy of the solution, the number of iterations $N_{\rm it}$ was set to be large enough so that for all values of r there is at least four digit agreement between $R_\alpha^{(N_{\rm it}+1)}(r)$ and $R_\alpha^{(N_{\rm it})}(r)$.

Equation (40) was solved several times by slowly varying the parameter Z until the corresponding ground-state total energy of helium is equal to the experimental value. The specific value of Z was found to be 1.99. Table I presents the total energies of the helium atom, where one electron is frozen in the $1s$ orbital while the other one is active. The calculated total energies of various states of helium are compared with the theoretical results of Abdurakhmanov *et al.* [50] and Slim *et al.* [18], and also with the measured values of Bashkin and Stoner [52]. Except for the ground state, all energies agree up to three digits in all of the aforementioned works.

For negative energies this system has a discrete set of solutions. For positive energies the equation has a continuous solution with a non-normalizable radial wave function. Therefore, as in the case of hydrogen, we construct wave packets using the helium continuum-state wave functions. We define

$$\phi_{il}(r) = \nu_{il} \int_{\kappa_{i-1}}^{\kappa_i} d\kappa\, R_{\kappa l}(r), \tag{42}$$

where ν_{il} is the normalization coefficient. Discretization points $\kappa_i, i = 1, \ldots, N_c$ and $E_{\rm max}$ are defined in a similar way as for hydrogen. Then the wave packets based on the two-electron helium wave functions are written as

$$\psi_\alpha^{\rm He}(\boldsymbol{r}_1, \boldsymbol{r}_2) = \psi_{1s}^{(Z)}(\boldsymbol{r}_2) \phi_{n_\alpha l_\alpha}(r_1) Y_{l_\alpha m_\alpha}(\hat{\boldsymbol{r}}_1) + \psi_{1s}^{(Z)}(\boldsymbol{r}_1) \phi_{n_\alpha l_\alpha}(r_2) Y_{l_\alpha m_\alpha}(\hat{\boldsymbol{r}}_2), \tag{43}$$

where the normalization coefficients are given as

$$\nu_{n_\alpha l_\alpha} = \left[2\left(\left\langle \phi_{n_\alpha l_\alpha} \middle| \phi_{n_\alpha l_\alpha} \right\rangle + \delta_{l_\alpha 0} \delta_{m_\alpha 0} \left\langle \phi_{n_\alpha l_\alpha} \middle| \phi_{1s}^{(Z)} \right\rangle \right) \right]^{-1/2} \tag{44}$$

and $\phi_{1s}^{(Z)}$ is the radial part of the function $\psi_{1s}^{(Z)}$.

Both the hydrogen and helium wave packets are referred to as bin states. Together with the eigenstates, they form the bases for the hydrogen and helium atoms. We note that the basis parameters $E_{\rm max}$ and $N_{\rm c}$ must be sufficiently large to obtain accurate cross sections. Their choice will be discussed later.

TABLE I. Total binding energy (in a.u.) of the helium atom in a specific state. Only the active orbital in the $(1snl)$ singlet states is listed in the first column.

State	Present	Ref. [50]	Ref. [18]	Expt. [52]
$1s$	−2.9040	−2.8725	−2.8655	−2.9036
$2s$	−2.1432	−2.1434	−2.1430	−2.1459
$3s$	−2.0605	−2.0606	−2.0604	−2.0613
$4s$	−2.0332	−2.0333	−2.0309	−2.0336
$2p$	−2.1223	−2.1224	−2.1224	−2.1239
$3p$	−2.0546	−2.0547	−2.0547	−2.0552
$4p$	−2.0308	−2.0309	−2.0307	−2.0311
$3d$	−2.0555	−2.0556	−2.0555	−2.0556

C. Matrix elements

In this section we reduce the matrix elements used in Eq. (19) into forms that are suitable for numerical evaluation by taking into account the definitions of the wave functions. When the direct matrix elements (20)–(22) are written in the integral form, we have exponential factors which can be reduced as follows:

$$(\boldsymbol{k}_\alpha - \boldsymbol{k}_{\alpha'})\boldsymbol{\sigma} = \boldsymbol{q}_\perp \boldsymbol{b} + (\varepsilon_{\alpha'} - \varepsilon_\alpha)t, \tag{45}$$

$$(\boldsymbol{k}_{1\beta} - \boldsymbol{k}_{1\beta'})\boldsymbol{\rho}_1 = \boldsymbol{q}_\perp \boldsymbol{b} + (\varepsilon_{\beta'} - \varepsilon_\beta)t, \tag{46}$$

$$(\boldsymbol{k}_{2\beta} - \boldsymbol{k}_{2\beta'})\boldsymbol{\rho}_1 = \boldsymbol{q}_\perp \boldsymbol{b} + (\varepsilon_{\beta'} - \varepsilon_\beta)t, \tag{47}$$

$$\boldsymbol{k}_{1\beta}\boldsymbol{\rho}_1 - \boldsymbol{k}_{2\beta'}\boldsymbol{\rho}_2 = \boldsymbol{q}_\perp \boldsymbol{b} + (\varepsilon_{\beta'} - \varepsilon_\beta)t, \tag{48}$$

$$\boldsymbol{k}_{2\beta}\boldsymbol{\rho}_1 - \boldsymbol{k}_{1\beta'}\boldsymbol{\rho}_2 = \boldsymbol{q}_\perp \boldsymbol{b} + (\varepsilon_{\beta'} - \varepsilon_\beta)t. \tag{49}$$

The exponential terms in the rearrangement matrix elements (23)–(26) can be written as

$$\boldsymbol{k}_\alpha\boldsymbol{\sigma}-\boldsymbol{k}_{1\beta'}\boldsymbol{\rho}_1=\boldsymbol{k}_\alpha\boldsymbol{\sigma}-\boldsymbol{k}_{2\beta'}\boldsymbol{\rho}_2=\boldsymbol{q}_\perp\boldsymbol{b}+\boldsymbol{q}_\parallel^{(1)}vt-\boldsymbol{v}\boldsymbol{r}_1, \quad (50)$$

$$\boldsymbol{k}_{1\beta}\boldsymbol{\rho}_1-\boldsymbol{k}_{\alpha'}\boldsymbol{\sigma}=\boldsymbol{k}_{2\beta}\boldsymbol{\rho}_1-\boldsymbol{k}_{\alpha'}\boldsymbol{\sigma}=\boldsymbol{q}_\perp\boldsymbol{b}+\boldsymbol{q}_\parallel^{(2)}vt+\boldsymbol{v}\boldsymbol{r}_1, \quad (51)$$

where $\boldsymbol{q}_\perp$ is the perpendicular component of the momentum transfer, which is the same in all transitions. The parallel components $\boldsymbol{q}_\parallel^{(1)}$ and $\boldsymbol{q}_\parallel^{(2)}$ depend on the transition states and are given as

$$\boldsymbol{q}_\parallel^{(1)}=\frac{v}{2}+\frac{\varepsilon_{\beta'}-\varepsilon_\alpha}{v}, \quad \boldsymbol{q}_\parallel^{(2)}=-\frac{v}{2}+\frac{\varepsilon_{\alpha'}-\varepsilon_\beta}{v}. \quad (52)$$

As $e^{\boldsymbol{q}_\perp\boldsymbol{b}}$ is the same in all matrix elements, it can be factored out and cancels when the matrix elements are inserted into Eq. (19). Therefore, we omit them but keep the original notations. Using these results and summing similar terms, the matrix elements (20)–(26) can be written in the forms

$$K^P_{\beta'\alpha}=\sqrt{2}\,e^{i(\epsilon_{\beta'}-\epsilon_\alpha)t}e^{iv^2t/2}\tilde{K}^B_{\beta'\alpha}, \quad (53)$$

$$K^T_{\alpha'\beta}=\sqrt{2}\,e^{i(\epsilon_{\alpha'}-\epsilon_\beta)t}e^{-iv^2t/2}\tilde{K}^A_{\alpha'\beta}, \quad (54)$$

$$L^P_{\beta'\beta}=\delta_{\beta',\beta}+e^{i(\epsilon_{\beta'}-\epsilon_\beta)t}\tilde{L}^P_{\beta'\beta}, \quad (55)$$

$$D^T_{\alpha'\alpha}=2\,e^{i(\epsilon_{\alpha'}-\epsilon_\alpha)t}\tilde{D}^T_{\alpha'\alpha}, \quad (56)$$

$$Q^P_{\beta'\alpha}=\sqrt{2}\,e^{i(\epsilon_{\beta'}-\epsilon_\alpha)t}e^{iv^2t/2}\tilde{Q}^P_{\beta'\alpha}, \quad (57)$$

$$Q^T_{\alpha'\beta}=\sqrt{2}\,e^{i(\epsilon_{\alpha'}-\epsilon_\beta)t}e^{-iv^2t/2}\tilde{Q}^T_{\alpha'\beta}, \quad (58)$$

$$D^P_{\beta'\beta}=e^{i(\epsilon_{\beta'}-\epsilon_\beta)t}\tilde{D}^P_{\beta'\beta}, \quad (59)$$

with

$$\tilde{K}^P_{\beta'\alpha}=\int d\boldsymbol{r}_1d\boldsymbol{r}_2\psi^{\mathrm{H}*}_{\beta'}(\boldsymbol{r}_1-\boldsymbol{R})\psi^{\mathrm{He}^+}_{1s}(\boldsymbol{r}_2)e^{-i\boldsymbol{v}\boldsymbol{r}_1}\psi^{\mathrm{He}}_\alpha(\boldsymbol{r}_1,\boldsymbol{r}_2), \quad (60)$$

$$\tilde{K}^T_{\alpha'\beta}=\int d\boldsymbol{r}_1d\boldsymbol{r}_2\psi^{\mathrm{He}*}_{\alpha'}(\boldsymbol{r}_1,\boldsymbol{r}_2)e^{i\boldsymbol{v}\boldsymbol{r}_1}\psi^{\mathrm{H}}_\beta(\boldsymbol{r}_1-\boldsymbol{R})\psi^{\mathrm{He}^+}_{1s}(\boldsymbol{r}_2), \quad (61)$$

$$\tilde{L}^P_{\beta'\beta}=\int d\boldsymbol{r}_1d\boldsymbol{r}_2\psi^{\mathrm{H}*}_{\beta'}(\boldsymbol{r}_2-\boldsymbol{R})\psi^{\mathrm{He}^+}_{1s}(\boldsymbol{r}_1)\times e^{-i\boldsymbol{v}\boldsymbol{r}_2}\psi^{\mathrm{H}}_\beta(\boldsymbol{r}_1-\boldsymbol{R})\psi^{\mathrm{He}^+}_{1s}(\boldsymbol{r}_2)e^{i\boldsymbol{v}\boldsymbol{r}_1}, \quad (62)$$

$$\tilde{D}^T_{\alpha'\alpha}=\int d\boldsymbol{r}_1d\boldsymbol{r}_2\psi^{\mathrm{He}*}_{\alpha'}(\boldsymbol{r}_1,\boldsymbol{r}_2)V_P\psi^{\mathrm{He}}_\alpha(\boldsymbol{r}_1,\boldsymbol{r}_2), \quad (63)$$

$$\tilde{Q}^P_{\beta'\alpha}=\int d\boldsymbol{r}_1d\boldsymbol{r}_2\psi^{\mathrm{H}*}_{\beta'}(\boldsymbol{r}_1-\boldsymbol{R})\psi^{\mathrm{He}^+}_{1s}(\boldsymbol{r}_2)e^{-i\boldsymbol{v}\boldsymbol{r}_1}\times\left[H_T-E^{\mathrm{He}}_\alpha+V_P\right]\psi^{\mathrm{He}}_\alpha(\boldsymbol{r}_1,\boldsymbol{r}_2), \quad (64)$$

$$\tilde{Q}^T_{\alpha'\beta}=\int d\boldsymbol{r}_1d\boldsymbol{r}_2\psi^{\mathrm{He}*}_{\alpha'}(\boldsymbol{r}_1,\boldsymbol{r}_2)e^{-i\boldsymbol{v}\boldsymbol{r}_1}\times\left[H_{P_1}-\varepsilon^{\mathrm{H}}_\beta+V_1\right]\psi^{\mathrm{H}}_\beta(\boldsymbol{r}_1-\boldsymbol{R})\psi^{\mathrm{He}^+}_{1s}(\boldsymbol{r}_2), \quad (65)$$

$$\tilde{D}^P_{\beta'\beta}=\int d\boldsymbol{r}_1d\boldsymbol{r}_2\psi^{\mathrm{H}*}_{\beta'}(\boldsymbol{r}_1-\boldsymbol{R})\psi^{\mathrm{He}^+}_{1s}(\boldsymbol{r}_2)V_1\psi^{\mathrm{H}}_\beta(\boldsymbol{r}_1-\boldsymbol{R})\psi^{\mathrm{He}^+}_{1s}(\boldsymbol{r}_2)+\int d\boldsymbol{r}_1d\boldsymbol{r}_2\psi^{\mathrm{H}*}_{\beta'}(\boldsymbol{r}_2-\boldsymbol{R})\psi^{\mathrm{He}^+}_{1s}(\boldsymbol{r}_1)e^{-i\boldsymbol{v}\boldsymbol{r}_2}\times\left[H_{P_1}-\varepsilon^{\mathrm{H}}_\beta+V_1\right]e^{i\boldsymbol{v}\boldsymbol{r}_1}\psi^{\mathrm{H}}_\beta(\boldsymbol{r}_1-\boldsymbol{R})\psi^{\mathrm{He}^+}_{1s}(\boldsymbol{r}_2), \quad (66)$$

where the vectors $\boldsymbol{x}_1$ and $\boldsymbol{x}_2$ were replaced with equivalent forms of $(\boldsymbol{r}_1-\boldsymbol{R})$ and $(\boldsymbol{r}_2-\boldsymbol{R})$, respectively.

In the direct matrix element $\tilde{D}^T$ and the first term of $\tilde{D}^P$ the terms with $(H_T-E^{\mathrm{He}}_\alpha)$ and $(H_P-\varepsilon^{\mathrm{H}}_\beta)$ vanish, since for both eigenstates and bin states we have

$$\left\langle\psi^{\mathrm{He}}_{\alpha'}\middle|H_T-E^{\mathrm{He}}_\alpha\middle|\psi^{\mathrm{He}}_\alpha\right\rangle=0, \quad \alpha',\alpha=1,\ldots,N, \quad (67)$$

$$\left\langle\psi^{\mathrm{H}}_{\beta'}\middle|H_P-\varepsilon^{\mathrm{H}}_\beta\middle|\psi^{\mathrm{H}}_\beta\right\rangle=0, \quad \beta',\beta=1,\ldots,M. \quad (68)$$

However, in the rearrangement matrix elements $\tilde{Q}^P$, $\tilde{Q}^T$ and in the second term of $\tilde{D}^P$, the terms containing $[H_T-E^{\mathrm{He}}_\alpha]\psi^{\mathrm{He}}_\alpha$ and $[H_P-\varepsilon^{\mathrm{H}}_\beta]\psi^{\mathrm{H}}_\beta$ remain, because the wave packets representing the continuum are not eigenstates. For a function

$$f(\boldsymbol{r})=\frac{1}{\sqrt{w}}\int_{\kappa_1}^{\kappa_2}d\kappa\,g_\kappa(\boldsymbol{r}), \quad (69)$$

where g_κ is an eigenfunction of an operator h, i.e.,

$$hg_\kappa(\boldsymbol{r})=\epsilon_\kappa g_\kappa(\boldsymbol{r})=\frac{\kappa^2}{2}g_\kappa(\boldsymbol{r}), \quad (70)$$

we have

$$[h-\varepsilon]f(\boldsymbol{r})=\frac{1}{\sqrt{w}}\int_{\kappa_{i-1}}^{\kappa_i}d\kappa\left(\frac{\kappa^2}{2}-\varepsilon\right)g_\kappa(\boldsymbol{r}). \quad (71)$$

Applying this to the positive-energy states of hydrogen and helium, we introduce

$$\chi^{\mathrm{H}}_\beta(\boldsymbol{r})=\left[H_P-\varepsilon^{\mathrm{H}}_\beta\right]\psi^{\mathrm{H}}_\beta(\boldsymbol{r})=\chi^{\mathrm{H}}_\beta(r)Y_{l_\beta m_\beta}(\hat{\boldsymbol{r}}), \quad (72)$$

with

$$\chi^{\mathrm{H}}_\beta(r)=\frac{1}{\sqrt{w_{n_\beta}}}\int_{\kappa_{n_\beta-1}}^{\kappa_{n_\beta}}d\kappa\left(\frac{\kappa^2}{2}-\varepsilon^{\mathrm{H}}_\beta\right)\phi^{\mathrm{H}}_{\kappa l_\beta}(r), \quad (73)$$

where $\epsilon^{\mathrm{H}}_\beta$ is the energy of the β state of hydrogen. Similarly, we introduce

$$\chi^{\mathrm{He}}_\alpha(\boldsymbol{r})=\chi^{\mathrm{He}}_\alpha(r)Y_{l_\alpha m_\alpha}(\hat{\boldsymbol{r}}), \quad (74)$$

with

$$\chi^{\mathrm{He}}_\alpha(r)=\frac{1}{\sqrt{w_{n_\alpha}}}\int_{\kappa_{n_\alpha-1}}^{\kappa_{n_\alpha}}d\kappa\left(\frac{\kappa^2}{2}-\varepsilon^{\mathrm{He}}_\alpha\right)\phi^{\mathrm{He}}_{\kappa l_\alpha}(r), \quad (75)$$

where $\varepsilon^{\mathrm{He}}_\alpha$ is the energy of the active helium electron in channel α. Consequently, we have

$$\begin{aligned}\left[H_T-E^{\mathrm{He}}_\alpha\right]\psi^{\mathrm{He}}_\alpha(\boldsymbol{r}_1,\boldsymbol{r}_2)&=\left[H_T-E^{\mathrm{He}}_\alpha\right]\left[\psi_\alpha(\mathbf{r}_1)\psi^{(Z)}_{1s}(\mathbf{r}_2)+\psi_\alpha(\mathbf{r}_2)\psi^{(Z)}_{1s}(\mathbf{r}_1)\right]\\&=\chi^{\mathrm{He}}_\alpha(\boldsymbol{r}_1)\psi^{(Z)}_{1s}(\boldsymbol{r}_2)+\chi^{\mathrm{He}}_\alpha(\boldsymbol{r}_2)\psi^{(Z)}_{1s}(\boldsymbol{r}_1).\end{aligned} \quad (76)$$

For eigenfunctions ψ^{H}_β and $\psi^{\mathrm{He}}_\alpha$, we have $\chi^{\mathrm{H}}_\beta=0$ and $\chi^{\mathrm{He}}_\alpha=0$.

Using the expansion of the helium wave function, the matrix elements can be written in forms that are convenient

for the calculations. The matrix elements $\tilde{K}^P_{\beta'\alpha}$, $\tilde{K}^T_{\alpha'\beta}$, and $\tilde{L}^P_{\beta'\beta}$ [Eqs. (60), (61), and (62), respectively] can be written as

$$\tilde{K}^P_{\beta'\alpha} = \langle \psi^{\mathrm{He}^+}_{1s} | \psi^{(Z)}_{1s} \rangle A\big[\psi^{\mathrm{H}}_{\beta'}, \psi_\alpha\big] + \langle \psi^{\mathrm{He}^+}_{1s} | \psi_\alpha \rangle A\big[\psi^{\mathrm{H}}_{\beta'}, \psi^{(Z)}_{1s}\big], \tag{77}$$

$$\tilde{K}^T_{\alpha'\beta} = \big(\tilde{K}^P_{\beta,\alpha'}\big)^*, \tag{78}$$

$$\tilde{L}^P_{\beta'\beta} = \delta_{\beta,\beta'} + A\big[\psi^{\mathrm{H}}_{\beta'}, \psi^{\mathrm{He}^+}_{1s}\big]\big(A\big[\psi^{\mathrm{H}}_{\beta}, \psi^{\mathrm{He}^+}_{1s}\big]\big)^*, \tag{79}$$

where

$$A[f, g] = \int d\boldsymbol{r}\, f^*(\boldsymbol{r} - \boldsymbol{R}) e^{-i\boldsymbol{v}\boldsymbol{r}} g(\boldsymbol{r}). \tag{80}$$

The rearrangement matrix elements (63)–(66) have more complex forms. These are written as

$$\tilde{Q}^P_{\beta'\alpha} = \frac{\tilde{K}^P_{\beta'\alpha}}{R} - \langle \psi^{\mathrm{He}^+}_{1s} | \psi^{(Z)}_{1s} \rangle A\big[\widetilde{\psi}^{\mathrm{H}}_{\beta'}, \psi_\alpha\big] - \langle \psi^{\mathrm{He}^+}_{1s} | \psi_\alpha \rangle A\big[\widetilde{\psi}^{\mathrm{H}}_{\beta'}, \psi^{(Z)}_{1s}\big] - D\big[\psi^{\mathrm{He}^+}_{1s}, \psi^{(Z)}_{1s}\big] A\big[\psi^{\mathrm{H}}_{\beta'}, \psi_\alpha\big] - D\big[\psi^{\mathrm{He}^+}_{1s}, \psi_\alpha\big] A\big[\psi^{\mathrm{H}}_{\beta'}, \psi^{(Z)}_{1s}\big]$$
$$+ \langle \psi^{\mathrm{He}^+}_{1s} | \psi^{(Z)}_{1s} \rangle A\big[\psi^{\mathrm{H}}_{\beta'}, \chi^{\mathrm{He}}_{\alpha}\big] + \langle \psi^{\mathrm{He}^+}_{1s} | \chi^{\mathrm{He}}_{\alpha} \rangle A\big[\psi^{\mathrm{H}}_{\beta'}, \psi^{(Z)}_{1s}\big], \tag{81}$$

$$\tilde{Q}^T_{\alpha'\beta} = \frac{\tilde{K}^T_{\alpha'\beta}}{R} - \big(\langle \psi^{\mathrm{He}^+}_{1s} | \psi^{(Z)}_{1s} \rangle A\big[\psi^{\mathrm{H}}_{\beta}, \widetilde{\psi}_{\alpha'}\big] + \langle \psi^{\mathrm{He}^+}_{1s} | \psi_{\alpha'} \rangle A\big[\psi^{\mathrm{H}}_{\beta}, \widetilde{\psi}^{(Z)}\big] + D\big[\psi^{\mathrm{He}^+}_{1s}, \psi^{(Z)}_{1s}\big] A\big[\psi^{\mathrm{H}}_{\beta}, \psi_{\alpha'}\big] + D\big[\psi^{\mathrm{He}^+}_{1s}, \psi_{\alpha'}\big] A\big[\psi^{\mathrm{H}}_{\beta}, \psi^{(Z)}_{1s}\big]$$
$$- A\big[\psi^{\mathrm{H}}_{\beta}, \psi_{\alpha'} D\big[\psi^{\mathrm{He}^+}_{1s}, \psi^{(Z)}_{1s}\big]\big] - A\big[\psi^{\mathrm{H}}_{\beta}, \psi^{(Z)}_{1s} D\big[\psi^{\mathrm{He}^+}_{1s}, \psi_{\alpha'}\big]\big] - \langle \psi^{\mathrm{He}^+}_{1s} | \psi^{(Z)}_{1s} \rangle A\big[\chi^{\mathrm{H}}_{\beta}, \psi_{\alpha'}\big] - \langle \psi^{\mathrm{He}^+}_{1s} | \psi_{\alpha'} \rangle A\big[\chi^{\mathrm{H}}_{\beta}, \psi^{(Z)}_{1s}\big]\big)^*, \tag{82}$$

where

$$D[f, g] = \int d\boldsymbol{r}\, f^*(\boldsymbol{r}) \left(\frac{1}{R} - \frac{1}{|\boldsymbol{R} - \boldsymbol{r}|}\right) g(\boldsymbol{r}) \tag{83}$$

and $\widetilde{\psi}(\boldsymbol{r}) = \psi(\boldsymbol{r})/r$.

For the direct matrix elements we have

$$\tilde{D}^T_{\alpha'\alpha} = D[\psi_{\alpha'}, \psi_\alpha] + \langle \psi^{(Z)}_{1s} | \psi_\alpha \rangle D\big[\psi_{\alpha'}, \psi^{(Z)}_{1s}\big] + \langle \psi_{\alpha'} | \psi^{(Z)}_{1s} \rangle D\big[\psi^{(Z)}_{1s}, \psi_\alpha\big] + \langle \psi_\alpha | \psi_{\alpha'} \rangle D\big[\psi^{(Z)}_{1s}, \psi^{(Z)}_{1s}\big], \tag{84}$$

$$\tilde{D}^P_{\beta'\beta} = \delta_{\beta,\beta'} D\big[\psi^{\mathrm{He}^+}_{1s}, \psi^{\mathrm{He}^+}_{1s}\big] + (-1)^{l_\beta + l_{\beta'}} D[\psi_{\beta'}, \psi_\beta] + B\big[\psi^{\mathrm{H}*}_{\beta'} \psi^{\mathrm{H}}_{\beta}, D\big[\psi^{\mathrm{He}^+}_{1s}, \psi^{\mathrm{He}^+}_{1s}\big]\big] + \frac{2}{R} A\big[\psi^{\mathrm{H}}_{\beta'}, \psi^{\mathrm{He}^+}_{1s}\big]\big(A\big[\psi^{\mathrm{H}}_{\beta}, \psi^{\mathrm{He}^+}_{1s}\big]\big)^*$$
$$- A\big[\widetilde{\psi}^{\mathrm{H}}_{\beta'}, \psi^{\mathrm{He}^+}_{1s}\big]\big(A\big[\psi^{\mathrm{H}}_{\beta}, \psi^{\mathrm{He}^+}_{1s}\big]\big)^* - A\big[\psi^{\mathrm{H}}_{\beta'}, \psi^{\mathrm{He}^+}_{1s}\big]\big(A\big[\psi^{\mathrm{H}}_{\beta}, \widetilde{\psi}^{\mathrm{He}^+}_{1s}\big]\big)^* + C_{\beta',\beta} + A\big[\chi^{\mathrm{H}}_{\beta'}, \psi^{\mathrm{He}^+}_{1s}\big]\big(A\big[\psi^{\mathrm{H}}_{\beta}, \psi^{\mathrm{He}^+}_{1s}\big]\big)^*, \tag{85}$$

where

$$B(f, g) = \int d\boldsymbol{r}\, f(\boldsymbol{r} - \boldsymbol{R}) g(\boldsymbol{r}), \tag{86}$$

$$C_{\beta',\beta} = \int d\boldsymbol{r_1} d\boldsymbol{r_2} \psi^{\mathrm{H}*}_{\beta'}(\boldsymbol{r}_1 - \boldsymbol{R}) e^{-i\boldsymbol{v}\boldsymbol{r}_1} \psi^{\mathrm{He}^+}_{1s}(\boldsymbol{r}_1) \psi^{\mathrm{H}}_{\beta}(\boldsymbol{r}_2 - \boldsymbol{R}) e^{i\boldsymbol{v}\boldsymbol{r}_2} \psi^{\mathrm{He}^+}_{1s}(\boldsymbol{r}_2) \frac{1}{|\boldsymbol{r}_1 - \boldsymbol{r}_2|}. \tag{87}$$

In our calculations of the matrix elements, the integral D was evaluated in spherical coordinates and all other integrals in spheroidal coordinates. Below we describe in some detail how to further simplify the most computationally demanding term, $C_{\beta',\beta}$. This term is a part of the matrix element that corresponds to the electron exchange process between the two possible final transfer channels β' and β containing the hydrogen atom and the He^+ ion. The term $|\boldsymbol{r}_1 - \boldsymbol{r}_2|^{-1}$ is expanded as

$$\frac{1}{|\boldsymbol{r}_1 - \boldsymbol{r}_2|} = 4\pi \sum_{\lambda\mu} \frac{1}{2\lambda + 1} U_\lambda(r_1, r_2) Y_{\lambda\mu}(\widehat{\boldsymbol{r}_1}) Y^*_{\lambda\mu}(\widehat{\boldsymbol{r}_2}), \tag{88}$$

where

$$U_\lambda(r_1, r_2) = \begin{cases} r_1^\lambda / r_2^{\lambda+1} & \text{for} \quad r_2 \geqslant r_1, \\ r_2^\lambda / r_1^{\lambda+1} & \text{for} \quad r_2 < r_1. \end{cases} \tag{89}$$

Then we have

$$C_{\beta',\beta} = \sum_{\lambda\mu} \frac{4\pi}{2\lambda + 1} \left[\int d\boldsymbol{r_1} d\boldsymbol{r_2} \psi^{\mathrm{H}*}_{\beta'}(\boldsymbol{r}_1 - \boldsymbol{R}) e^{-i\boldsymbol{v}\boldsymbol{r}_1} \psi^{\mathrm{He}^+}_{1s}(\boldsymbol{r}_1) \psi^{\mathrm{H}}_{\beta}(\boldsymbol{r}_2 - \boldsymbol{R}) e^{i\boldsymbol{v}\boldsymbol{r}_2} \psi^{\mathrm{He}^+}_{1s}(\boldsymbol{r}_2) U_\lambda(r_1, r_2) Y^*_{\lambda\mu}(\widehat{\boldsymbol{r}_1}) Y_{\lambda\mu}(\widehat{\boldsymbol{r}_2}) \right]$$
$$= \sum_{\lambda\mu} \frac{1}{2\lambda + 1} \left[\int d\boldsymbol{r_1} \psi^{\mathrm{H}*}_{\beta'}(\boldsymbol{r}_1 - \boldsymbol{R}) e^{-i\boldsymbol{v}\boldsymbol{r}_1} \phi_0(r_1) Y_{\lambda\mu}(\widehat{\boldsymbol{r}_1}) \int d\boldsymbol{r_2} \psi^{\mathrm{H}}_{\beta}(\boldsymbol{r}_2 - \boldsymbol{R}) e^{i\boldsymbol{v}\boldsymbol{r}_2} \phi_0(r_2) Y^*_{\lambda\mu}(\widehat{\boldsymbol{r}_2}) U_\lambda(r_1, r_2) \right], \tag{90}$$

where ϕ_0 is the radial part of $\psi_{1s}^{\mathrm{He}^+}$. In our calculations we use spheroidal coordinates, where the integral is reduced to a four-dimensional entity. Generally, this integral can be evaluated for all channels, but the calculations are extremely time consuming. Also, including them in the calculations does not change the results considerably provided the collision energy is not too small. Therefore, we include only the $C_{1s,1s}$ term and neglect all others. This approximation imposes a lower limit to the incident energy below which the results may deteriorate. No further approximations were used in the numerical evaluations of all other direct and rearrangement matrix elements.

III. DETAILS OF THE CALCULATIONS

A. Cross sections

Once the matrix elements have been calculated, the system of differential equations (19) can be solved to obtain the transition amplitudes $a_\alpha(+\infty, \boldsymbol{b})$ and $b_\beta(+\infty, \boldsymbol{b})$ for the required range of impact parameters b. The probability to find the system in the direct-scattering channel α and the rearrangement channel β after the collision is found as

$$P_\alpha(b) = |a_\alpha(+\infty, \boldsymbol{b})|^2, \quad P_\beta(b) = |b_\beta(+\infty, \boldsymbol{b})|^2. \tag{91}$$

The partial cross sections for the transition to states α and β are calculated as

$$\sigma_\alpha = 2\pi \int_0^{b_{\max}} db\, b\, P_\alpha(b), \quad \sigma_\beta = 2\pi \int_0^{b_{\max}} db\, b\, P_\beta(b), \tag{92}$$

where $b_{\max}$, the upper limit for the impact parameter, is chosen to be sufficiently high, as will be detailed below. The total electron-capture cross section is the sum of the cross sections for transitions into the negative-energy eigenstates of hydrogen:

$$\sigma_{\mathrm{tot}}^{\mathrm{capt}} = \sum_{\beta, \epsilon_\beta < 0} \sigma_\beta. \tag{93}$$

The total single-ionization cross section is the sum of the partial cross sections for excitation of the positive-energy pseudostates of the target and electron transfer into the continuum of hydrogen:

$$\sigma_{\mathrm{tot}}^{\mathrm{ion}} = \sum_{\alpha, \epsilon_\alpha > 0} \sigma_\alpha + \sum_{\beta, \epsilon_\beta > 0} \sigma_\beta. \tag{94}$$

In order to estimate double ionization of helium we use an independent-event model. In the IEM, the process is modeled as a combination of two independent processes: single ionization of helium and subsequent ionization of the helium ion. Accordingly, the double-ionization probability is the product of the two individual ionization probabilities. The total probabilities for single ionization of helium and ionization of the helium ion are found as

$$P_{\mathrm{ion}}^{\mathrm{He}}(b) = \sum_{\alpha, \epsilon_\alpha > 0} P_\alpha(b) + \sum_{\beta, \epsilon_\beta > 0} P_\beta(b), \tag{95}$$

$$P_{\mathrm{ion}}^{\mathrm{He}^+}(b) = \sum_{\gamma, \epsilon_\gamma > 0} P_\gamma(b) + \sum_{\xi, \epsilon_\xi > 0} P_\xi(b), \tag{96}$$

where P_γ and P_ξ are the probabilities for direct ionization of the helium ion and electron capture into the continuum of hydrogen, respectively, in $p + \mathrm{He}^+$ collisions. Finally, the double-ionization cross section is calculated as

$$\sigma = 2\pi \int_0^{b_{\max}} db\, b\, P_{\mathrm{ion}}^{\mathrm{He}}(b) P_{\mathrm{ion}}^{\mathrm{He}^+}(b). \tag{97}$$

We present the total electron capture as well as the single- and double-ionization cross sections for energies within the range from 15 keV to 1 MeV. In order to test our computer code, we first calculated the electron-capture cross section using the first Born approximation. We obtained good agreement with the results of Belkić [6]. The agreement was within 5% for all energies considered here.

B. Convergence studies

Our predictions depend on several factors, such as the accuracy of the helium wave functions and corresponding energy levels, as well as the accuracy of the matrix elements. We investigate the dependence of the resulting cross sections on the number of bins N_c, the maximum energy of the ejected electron $E_{\max}$, and the maximum angular-momentum quantum number $l_{\max}$ of the states included. A number of calculations were performed to test the convergence of the predicted cross sections in terms of the number of both target-centered and projectile-centered states. For simplicity we used the same number of basis functions for the target and projectile. We systematically increased the number of states to obtain convergent results while thoroughly checking the accuracy of the employed wave functions for the projectile- and target-centered states.

For given N_c and $l_{\max}$, the total number of states is found as

$$N = \sum_{l=0}^{l_{\max}} (n_{\max} + N_c - l)(2l + 1), \tag{98}$$

where $n_{\max}$ is the maximum principal quantum number of eigenstates. Our calculations show that $n_{\max} = 5$ is sufficient. As mentioned above, the resulting cross sections also depend on the choice of $b_{\max}$, the upper limit for the impact parameter. In our calculations we set $b_{\max} = 10$. Increasing this parameter further had no significant effect on the final results.

The convergence of the cross sections in terms of the number of bin states is shown in Fig. 2, where the number of bins were increased up to $N_c = 20$, at energies 50 keV, 100 keV, 500 keV, and 1 MeV, respectively. Calculations were performed with fixed values $n_{\max} = 5$ and $l_{\max} = 3$. Both the electron-capture (upper panel) and ionization (lower panel) results appear sufficiently converged. Both for electron capture and ionization, the difference between the cross sections calculated with $N_c = 16$ and $N_c = 20$ is less than 0.5% for all energies. Including positive-energy pseudostates is not only important to obtain an accurate ionization cross section but also improves the electron-capture cross section. This can be seen in the upper panel of Fig. 2. Similar conclusions were drawn by Slim *et al.* [18]. The ionization cross sections are particularly sensitive to the number of positive-energy pseudostates and the density of the continuum discretization. To get accurate results and better convergence in terms of

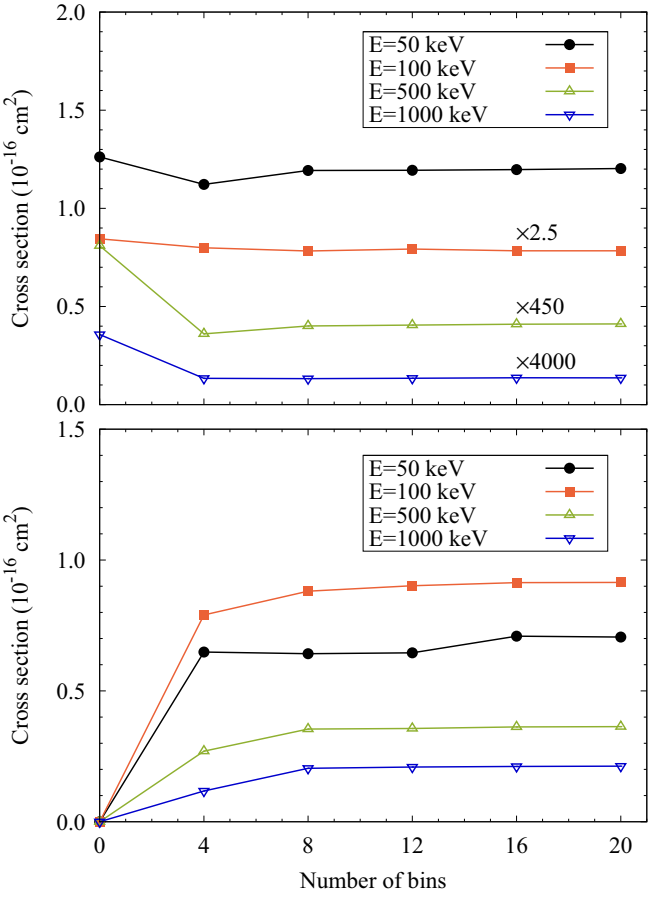

FIG. 2. Convergence of the present results with respect to the number of bin states N_c for the predicted total cross sections for electron capture (upper panel) and single ionization (lower panel) in p-He collisions. The four lines (connecting the points to guide the eye) represent the cross sections at the incident proton energies of 50 keV, 100 keV, 500 keV, and 1 MeV, respectively. Note that $N_c = 0$ yields no ionization cross section due to the lack of positive-energy states.

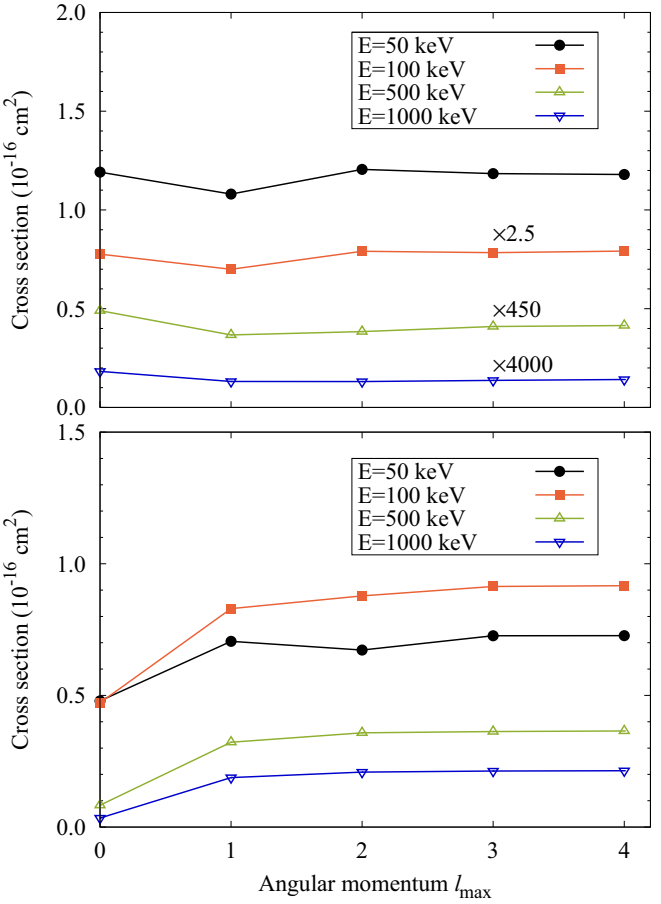

FIG. 3. Convergence of the present results as a function of l_{max} for the predicted total cross sections for electron capture (upper panel) and single ionization (lower panel) in p-He collisions. The four lines (connecting the points to guide the eye) represent the cross sections at the incident proton energies of 50 keV, 100 keV, 500 keV, and 1 MeV, respectively. The number of bins was set to $N_c = 20$.

positive-energy pseudostates, the maximum energy of the included bin states, E_{max}, needs to be large enough. In our calculations depending on the projectile energy, $k_{max}(=\sqrt{2E_{max}})$ ranged from 3.5 for the lower energies to 7.5 for the higher energies. The parameter was checked for each energy individually.

Next, we investigate the convergence of the electron-capture and ionization cross sections in terms of the maximum allowed orbital quantum number l_{max}. The results are presented in Fig. 3 for l_{max} ranging from zero to 4 at energies of 50 keV, 100 keV, 500 keV, and 1 MeV. Both electron-capture (upper panel) and ionization (lower panel) cross sections appear converged in terms of l_{max} too. In general, convergence was achieved with $l_{max} = 3$ for all energies considered.

IV. RESULTS

As discussed above, setting $n_{max} = 5$, $l_{max} = 3$, and $N_c = 20$ was required to obtain sufficiently accurate results. The basis with these parameters consists of the 366 target- and projectile-centered functions. Below we present our main results for the integrated cross sections.

A. Electron capture and excitation

Our results for the total electron-capture cross section as a function of incident energy are presented in Fig. 4 in comparison with the experimental data and the results of other theoretical works. As mentioned before, the total electron-capture cross section is the sum of the cross sections for the transitions into all negative-energy states of hydrogen. Capture into the 1s state provides the dominant contribution. The total electron-capture cross section reaches its peak around 25 keV. As seen from the figure, we obtained good agreement with the experimental data of Shah and Gilbody [36] and Shah *et al.* [37], except for the energy range of 30–100 keV, where our calculated cross sections exceed their data by about 15%. In this energy range only the results of Baxter and Kirchner [5] agree with the measurements of Shah *et al.* [37], while the results of all other calculations are slightly higher, most likely due to the frozen-core approximation used to treat the target structure. It is also interesting to compare our results with

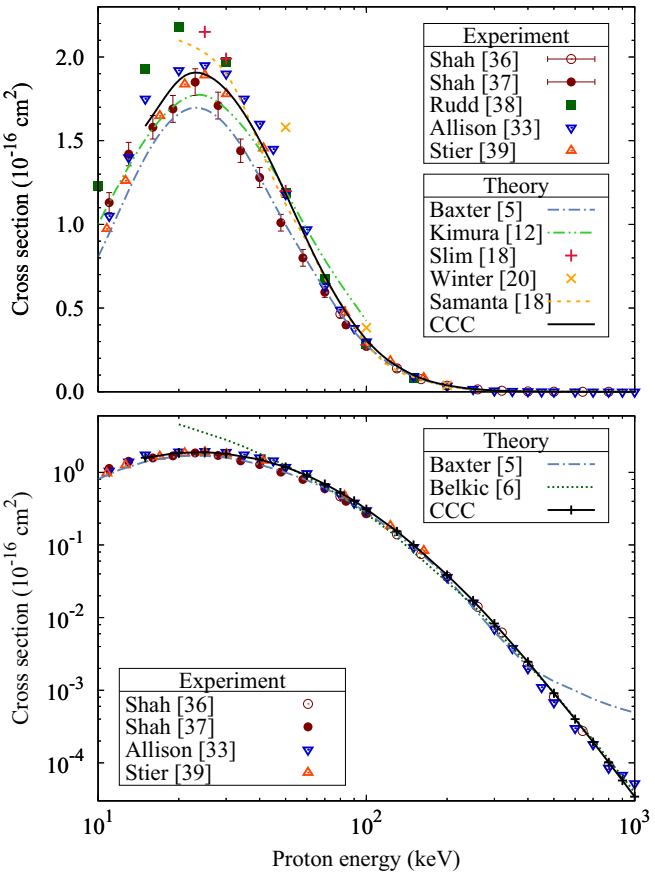

FIG. 4. Total cross section for electron capture in $p + \mathrm{He}(1s^2)$ collisions as a function of the incident proton energy (top and bottom panels linear and log scales, respectively). The present CCC results are represented by the black solid line. The experimental data are due to Shah and Gilbody [36], Shah *et al.* [37], Rudd *et al.* [38], Allison [33], Stier and Barnett [39]. The other theoretical results are from Baxter and Kirchner [5], Kimura and Lin [12], Slim *et al.* [18], Winter [20], Samanta and Purkait [17], Belkić [6].

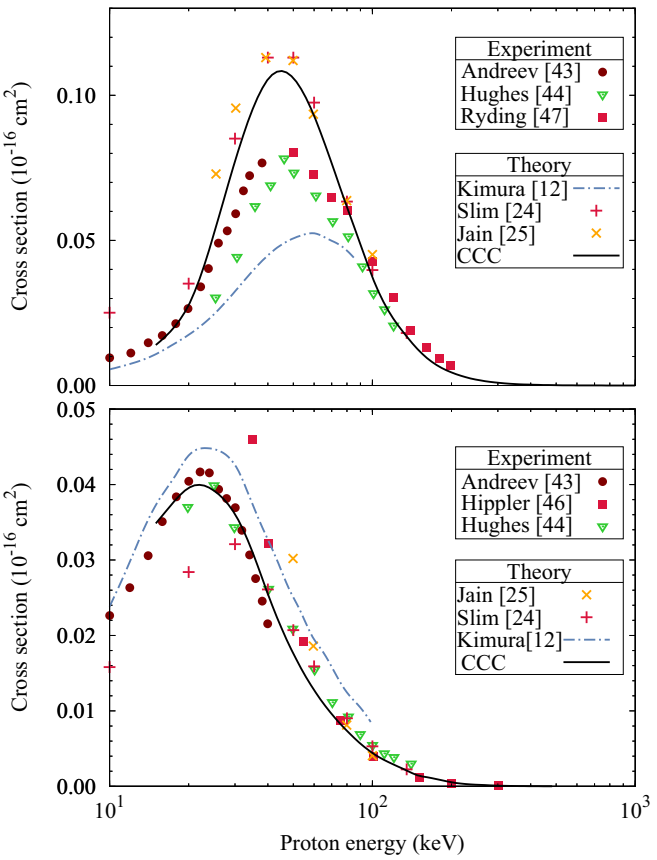

FIG. 5. Cross sections for electron capture into the $2s$ (upper panel) and $2p$ (lower panel) states of hydrogen in $p + \mathrm{He}(1s^2)$ collisions. The CCC results are represented by the black solid line. The experimental data are due to Andreev *et al.* [43], Hughes *et al.* [44], Hippler *et al.* [46], Ryding *et al.* [47]. The other theoretical results are from Kimura and Lin [12], Slim *et al.* [24], Jain *et al.* [25].

the close-coupling calculations of Winter [20] and Slim *et al.* [18]. Winter neglected electron exchange in the final transfer channel and the calculations included only 50 Sturmian basis functions. The result of Winter [20] exceeds ours by 30% at 50 keV but agrees at 200 keV. Slim *et al.* [18] succeeded to include electron exchange in the transfer channel, even though they used only 51 basis functions. Their electron-capture results exceed the CCC predictions by about 15% at 25 keV and 30 keV, but agree for the higher energies. Measurements by Stier and Barnett [39], Allison [33], and Rudd *et al.* [38] are also shown; however, these include the transfer ionization cross section in addition to electron capture with the second electron staying bound.

In the lower panel of Fig. 4, the same results are given on a logarithmic y scale to highlight the higher-energy region. In the energy range from 100 keV to 1 MeV, our calculations agree well with the experimental results of Shah and Gilbody [36]. The theoretical results of Baxter and Kirchner [5] are also in good agreement with the experimental data up to 400 keV, whereas they deviate from the data and other calculations at the higher energies. In this energy range the B1B calculations of Belkić [6], using the Roothaan-Hartree-Fock wave functions, also yield excellent agreement with the experimental data.

Electron capture into the $1s$ state of hydrogen dominates the charge-transfer process, but captures into other channels are also worth investigating. In Fig. 5 we present the partial cross sections for electron capture into the $n = 2$ shell of hydrogen. At the lower and higher energies the CCC results for electron capture into the $2s$ state agree with the experimental data. However, a clear discrepancy between the experimental and theoretical results is seen in the intermediate energy range, where the CCC results are in good agreement with the calculations of Slim *et al.* [24] and Jain *et al.* [25], but exceed the experimental data. For electron capture into the $2p$ state we observe fairly good agreement with the cross sections obtained experimentally, except for the results of Hippler and Schartner [45], which exceed other results at the intermediate energy range.

In Fig. 6 we provide the cross sections for direct excitation of helium into the $2p$ state and the sum of the cross sections for excitation into the $2s$ and $2p$ states of helium. We obtained agreement with the experimental data of Park and Schowengerdt [48] for both of these calculations in the

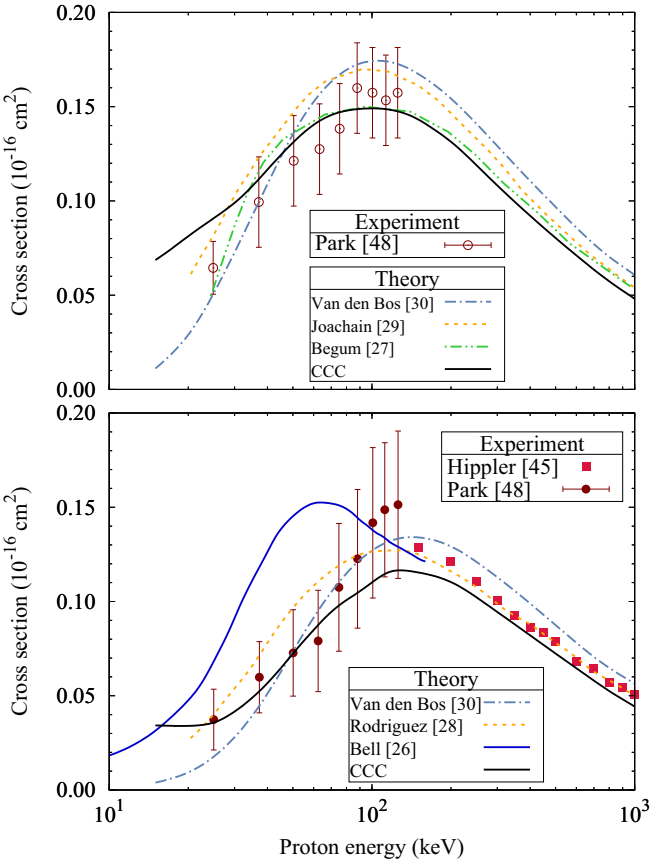

FIG. 6. Sum of cross sections for target excitation into the $2s$ and $2p$ states (upper panel) and cross section for excitation into the $2p$ state (lower panel) of helium in $p + \mathrm{He}(1s^2)$ collisions. The CCC results are represented as a black solid line. The experimental data are due to Hippler and Schartner [45], Park and Schowengerdt [48]. The other theoretical results are from Begum *et al.* [27], Joachain and Vanderpoorten [29], van den Bos [30].

lower and intermediate energy regions. The CCC results for excitation of helium into the $2p$ state lie slightly below the experimental data and other theoretical results above 150 keV, the difference with experiment being within 10%. The sum of the calculated cross sections for excitation into the $2s$ and $2p$ states is in good agreement with the results of Begum *et al.* [27] in the intermediate energy range. At the higher energies our results are below all the other theories, including the calculations by van den Bos [30] and Joachain and Vanderpoorten [29].

B. Ionization

In Fig. 7 the total single-ionization cross section is compared with the experimental data [36,37] and other calculations [5,9,18,20]. It can be seen that the ionization cross section reaches a maximum around 100 keV and decreases almost linearly with increasing energy of the projectile. On the other hand, as we have observed in the previous section, the electron-capture cross section falls off exponentially after reaching its maximum near 25 keV. The CCC results for single ionization exceed the experimental data of Shah and

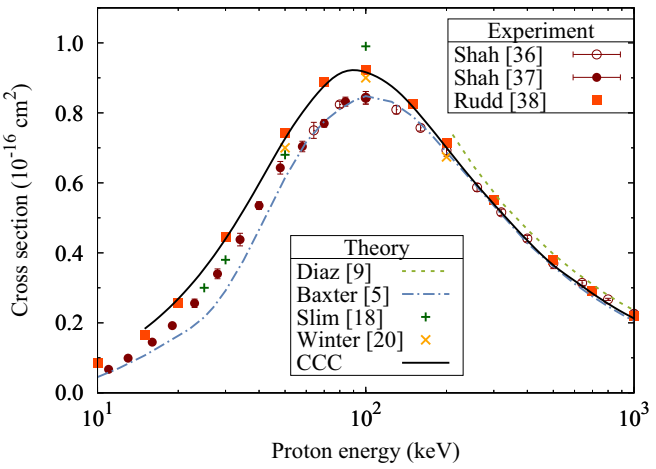

FIG. 7. Cross section for single ionization in $p + \mathrm{He}(1s^2)$ collisions as a function of incident energy. The CCC results are represented by the black solid line. The experimental data are due to Shah and Gilbody [36], Shah *et al.* [37], Rudd *et al.* [38]. The other theoretical results are from Baxter and Kirchner [5], Díaz *et al.* [9], Slim *et al.* [18], Winter [20].

Gilbody [36] and Shah *et al.* [37] by about 10% below 200 keV. The calculations of Baxter and Kirchner [5] based on the time-dependent density-functional theory, where the Wilken and Bauer model is applied, agree with the experiments except for the lower energies. Below 60 keV their results lie slightly below the data. Experimental data of Rudd *et al.* [38] that include double ionization in addition to single ionization are also shown. As we will see later, the double ionization cross section is very small and cannot explain the difference between the data of Shah and Gilbody [36], Shah *et al.* [37], and Rudd *et al.* [38].

Our results are in fair agreement with the close-coupling calculations by Winter [20]. The results of Slim *et al.* [18], which take into account electron exchange in the final states, exceed the experimental data as well as the CCC calculations at 100 keV. Above 200 keV all theoretical predictions, including ours, and the experimental data agree very well with each other, with the exception of the results of Díaz *et al.* [9], which are moderately higher. Note that employing a more accurate multicore description of the helium target will likely result in a reduction of the theoretical cross sections [21].

In Fig. 8 we present our results for double ionization, as obtained with the IEM model. Below 40 keV we observe good agreement with experiment, but for the higher energies our cross sections significantly exceed the measured data. Significantly larger double-ionization cross sections were also obtained in IEM calculations by Baxter and Kirchner [5], Kumar and Roy [32], and Ford and Reading [31]. The present results and those of all displayed IEM calculations are overall in reasonable agreement with each other. The observed large discrepancy with experiment suggests that there exists a strong correlation between one- and two-electron processes as far as double ionization of helium is concerned. In other words, the representation of double ionization using the IEM does not seem appropriate.

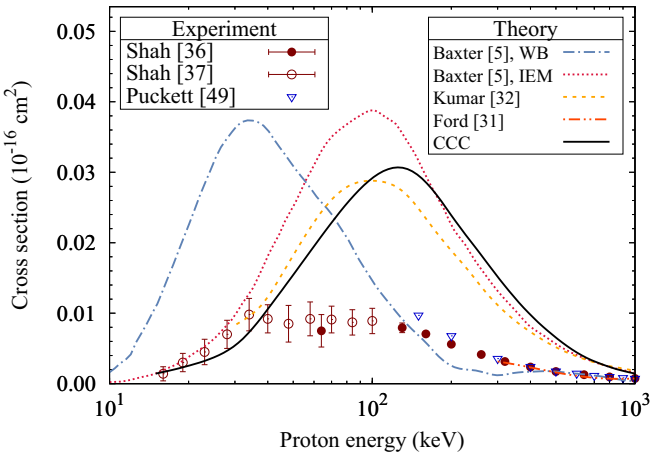

FIG. 8. Cross section for double ionization of helium in $p+$ He($1s^2$) collisions as a function of incident energy. The CCC results are represented by the black solid line. The experimental data are due to Shah and Gilbody [36], Shah *et al.* [37], Puckett and Martin [49]. The other theoretical results are from Ford and Reading [31], Kumar and Roy [32], Baxter and Kirchner [5].

V. SUMMARY AND CONCLUSIONS

To summarize, we investigated the four-body problem of proton collisions with helium using the semiclassical convergent close-coupling method. The wave-packet approach was applied to discretize the continuum both for the target and the projectile. The target was treated as a three-body system, where the electron-correlation effects were fully taken into account. We assumed that one of the helium electrons is frozen in the $1s$ orbital of He^+ throughout the collision. The target states were described by parameter-dependent wave functions, with the parameter fixed in such a way that the calculated ground-state energy of the active electron matches the measured value. With this modification, all calculated energy levels of the active electron of helium are in excellent agreement with the corresponding experimental values. The predicted cross sections were found to be sensitive to the target description, and using more accurate energy levels considerably improved the results of our calculations.

We studied the convergence of the results in terms of the number of basis functions and the maximum allowed orbital angular momentum of the included states at several energies of the projectile. Having obtained very satisfactory convergence, the total electron-capture and single-ionization cross sections were calculated in the energy range from 15 keV to 1 MeV.

There are many experiments and theoretical results available for these processes for comparison. We note that some discrepancies exist among them below 150 keV. In this energy range the agreement between our calculations and the experimental data of Shah and Gilbody [36] and Shah *et al.* [37] is within 15% for both electron capture and single ionization. Above 150 keV our results and all experiments agree very well. It is worth mentioning that among the close-coupling calculations for electron capture, the CCC results are in better agreement with experiment. This is likely due to the more accurate target description and the size of the basis applied.

Apart from the total cross sections, we investigated transfer cross sections into the $2s$ and $2p$ states of hydrogen, and excitation into the $2s$ and $2p$ states of helium. Fair agreement with other works was obtained in these particular cases as well. Furthermore, we used the independent-event model to study double ionization of the target, where double ionization is formulated as a combination of two independent processes: single ionization of helium and sequential ionization of the resulting helium ion by proton impact. Except for the lower energies, however, we failed to get agreement with the experimental data. The same idea can be used to describe other two-electron processes such as double capture, simultaneous transfer and ionization and double excitation. However, the validity of the independent-event model is not always guaranteed. On the other hand, the WP-CCC method can be used to develop a more sophisticated approach to the two-electron processes; however, this is beyond the scope of the present paper.

In this work we discretized the continuum using the wave-packet method. An advantage of this method is that it allows us to study electrons ejected with arbitrary energies easily. This is done by changing the number of bins and the maximum allowed energy of the ejected electrons. Therefore, this approach can be applied to study differential ionization. Specifically, the partial cross sections for transfer into all positive-energy channels that we calculated can be used to obtain differential cross sections for ionization of helium. Calculations of the fully and doubly differential cross sections for single ionization of the helium atom by proton and C^{6+} impact are currently underway. The previous study of C^{6+} impact single ionization of He using the one-center fully quantum-mechanical CCC approach [53] revealed a significant disagreement with the measurements of Schulz *et al.* [54] for the fully differential cross section in the perpendicular plane. We are now in a position to revisit this problem using a more accurate two-center approach.

ACKNOWLEDGMENTS

This work was supported by the Australian Research Council, the Pawsey Supercomputer Centre, and the National Computing Infrastructure. We also acknowledge partial support from the United States National Science Foundation under Grants No. PHY-1415656 (A.S.K.), No. PHY-1403245 (K.B.), and No. PHY-1803844 (K.B.).

[1] D. Tseliakhovich, C. M. Hirata, and K. Heng, Mon. Not. R. Astron. Soc. **422**, 2357 (2012).
[2] O. Marchuk, Phys. Scr. **89**, 114010 (2014).
[3] D. Belkić, J. Math. Chem. **47**, 1366 (2010).
[4] G. V. Avakov, A. R. Ashurov, L. D. Blokhintsev, A. S. Kadyrov, A. M. Mukhamedzhanov, and M. V. Poletayeva, J. Phys. B **23**, 4151 (1990).
[5] M. Baxter and T. Kirchner, Phys. Rev. A **93**, 012502 (2016).

[6] D. Belkić, Phys. Rev. A **37**, 55 (1988).
[7] B. H. Bransden and L. T. S. F. Lam, Proc. Phys. Soc. **87**, 653 (1966).
[8] G. R. Deco, J. M. Maidagan, and R. D. Rivarola, J. Phys. B **17**, L707 (1984).
[9] C. Díaz, F. Martín, and A. Salin, J. Phys. B **33**, 4373 (2000).
[10] T. A. Green, H. E. Stanley, and Y. C. Chiang, Helv. Phys. Acta **38**, 109 (1965).
[11] S. Jana, C. R. Mandal, and M. Purkait, J. Phys. B **48**, 045203 (2015).
[12] M. Kimura and C. D. Lin, Phys. Rev. A **34**, 176 (1986).
[13] I. Mancev, V. Mergel, and L. Schmidt, J. Phys. B **36**, 2733 (2003).
[14] R. A. Mapleton, Phys. Rev. **122**, 528 (1961).
[15] P. J. Schultz and K. G. Lynn, Rev. Mod. Phys. **60**, 701 (1988).
[16] M. Rahmanian, F. Shojaei, and R. Fathi, Eur. Phys. J. D **70**, 241 (2016).
[17] R. Samanta and M. Purkait, Phys. Scr. **84**, 065301 (2011).
[18] H. A. Slim, E. L. Heck, B. H. Bransden, and D. R. Flower, J. Phys. B **24**, L421 (1991).
[19] N. Toshima, T. Ishihara, and J. Eichler, Phys. Rev. A **36**, 2659 (1987).
[20] T. G. Winter, Phys. Rev. A **44**, 4353 (1991).
[21] X. Guan and K. Bartschat, Phys. Rev. Lett. **103**, 213201 (2009).
[22] D. Zajfman and D. Maor, Phys. Rev. Lett. **56**, 320 (1986).
[23] M. Zapukhlyak, T. Kirchner, A. Hasan, B. Tooke, and M. Schulz, Phys. Rev. A **77**, 012720 (2008).
[24] H. A. Slim, E. L. Heck, B. H. Bransden, and D. R. Flower, J. Phys. B **24**, 1683 (1991).
[25] A. Jain, C. D. Lin, and W. Fritsch, Phys. Rev. A **36**, 2041 (1987).
[26] R. J. Bell, Proc. Phys. Soc. **78**, 903 (1961).
[27] S. Begum, B. H. Bransden, and J. Coleman, J. Phys. B **6**, 837 (1973).
[28] V. D. Rodríguez, C. A. Ramírez, R. D. Rivarola, and J. E. Miraglia, Phys. Rev. A **55**, 4201 (1997).
[29] J. Joachain and R. Vanderpoorten, J. Phys. B **7**, 817 (1974).
[30] J. van den Bos, Phys. Rev. **181**, 191 (1969).
[31] A. L. Ford and J. F. Reading, J. Phys. B **27**, 4215 (1994).
[32] A. Kumar and B. N. Roy, J. Phys. B **10**, 3047 (1977).
[33] S. K. Allison, Rev. Mod. Phys. **30**, 1137 (1958).
[34] F. D. Heer, J. Schutten, and H. Moustafa, Physica **32**, 1766 (1966).
[35] E. Horsdal-Pedersen, C. L. Cocke, and M. Stockli, Phys. Rev. Lett. **50**, 1910 (1983).
[36] M. B. Shah and H. B. Gilbody, J. Phys. B **18**, 899 (1985).
[37] M. B. Shah, P. McCallion, and H. B. Gilbody, J. Phys. B **22**, 3037 (1989).
[38] M. E. Rudd, R. D. DuBois, L. H. Toburen, C. A. Ratcliffe, and T. V. Goffe, Phys. Rev. A **28**, 3244 (1983).
[39] P. M. Stier and C. F. Barnett, Phys. Rev. **103**, 896 (1956).
[40] L. H. Toburen, M. Y. Nakai, and R. A. Langley, Phys. Rev. **171**, 114 (1968).
[41] L. M. Welsh, K. H. Berkner, S. N. Kaplan, and R. V. Pyle, Phys. Rev. **158**, 85 (1967).
[42] J. F. Williams and D. N. F. Dunbar, Phys. Rev. **149**, 62 (1966).
[43] E. P. Andreev, V. A. Ankudinov, and S. V. Bobashev, Sov. Phys. JETP **23**, 375 (1966).
[44] R. H. Hughes, C. A. Stigers, B. M. Doughty, and E. D. Stokes, Phys. Rev. A **1**, 1424 (1970).
[45] R. Hippler and K. H. Schartner, J. Phys. B **7**, 618 (1974).
[46] R. Hippler, W. Harbich, M. Faust, H. O. Lutz, and L. J. Dube, J. Phys. B **19**, 1507 (1986).
[47] G. Ryding, A. B. Wittkower, and H. B. Gilbody, Proc. Phys. Soc. **89**, 547 (1966).
[48] J. T. Park and F. D. Schowengerdt, Phys. Rev. **185**, 152 (1969).
[49] L. J. Puckett and D. W. Martin, Phys. Rev. A **1**, 1432 (1970).
[50] I. B. Abdurakhmanov, A. S. Kadyrov, I. Bray, and K. Bartschat, Phys. Rev. A **96**, 022702 (2017).
[51] I. B. Abdurakhmanov, A. S. Kadyrov, and I. Bray, Phys. Rev. A **94**, 022703 (2016).
[52] S. Bashkin and J. Stoner, *Atomic Energy Levels and Grotrian Diagrams* (North-Holland Publishing Company, Amsterdam, 1975), Vol. 1.
[53] I. B. Abdurakhmanov, I. Bray, D. V. Fursa, A. S. Kadyrov, and A. T. Stelbovics, Phys. Rev. A **86**, 034701 (2012).
[54] M. Schulz, R. Moshammer, D. Fischer, H. Kollmus, D. H. Madison, S. Jones, and J. Ullrich, Nature (London) **422**, 48 (2003).